

---

# Uncertainty Prediction for Deep Sequential Regression Using Meta Models

---

Jiří Navrátil<sup>1</sup> Matthew Arnold<sup>1</sup> Benjamin Elder<sup>1</sup>

## Abstract

Generating high quality uncertainty estimates for sequential regression, particularly deep recurrent networks, remains a challenging and open problem. Existing approaches often make restrictive assumptions (such as stationarity) yet still perform poorly in practice, particularly in presence of real world non-stationary signals and drift. Using the concept of meta-modeling, we describe a flexible method that can generate symmetric and asymmetric uncertainty estimates, makes no assumptions about stationarity, and outperforms competitive baselines on both drift and non drift scenarios. This work helps make sequential regression more effective and practical for use in real-world applications, and is a powerful new addition to the modeling toolbox for sequential uncertainty quantification in general.

## 1. Introduction

The ability to quantify the uncertainty of a model is one of the fundamental requirements in trusted, safe, and actionable AI (Arnold et al., 2019; Jiang et al., 2018; Begoli et al., 2019).

This paper focuses on uncertainty quantification in regression tasks, particularly in the context of deep neural networks (DNN). We define a sequential task as one involving an ordered series of input elements, represented by features, and an ordered series of outputs. In sequential *regression* tasks (SRT), the output elements are (possibly multivariate) real-valued variables. SRT occur in numerous applications, among others, in weather modeling, environmental modeling, energy optimization, and medical applications. When the cost of making an incorrect prediction is particularly high, such as in human safety, models without a reliable uncertainty estimation are perceived high risk and may not be adopted.

Uncertainty prediction in DNNs has been subject to ac-

<sup>1</sup>IBM Thomas J. Watson Research Center, Yorktown Heights, NY, USA. Correspondence to: Jiří Navrátil <jiri@us.ibm.com>.

tive research, in particular, spurred by what has become known as the “Overconfidence Problem” of DNNs (Guo et al., 2017), and by their susceptibility to adversarial attacks (Madry et al., 2017). However, the bulk of work is concerned with non-sequential, classification tasks (see Section 2) leaving a noticeable gap for SRT.

In this paper we introduce a meta-modeling concept as an approach to achieving high-quality uncertainty quantification in DNNs for SRT. We demonstrate that it not only outperforms competitive baselines but also provides consistent results across a variety of drift scenarios. We believe the approach represents a new powerful addition to the modeling toolbox in general.

The novel contributions of this paper are summarized as follows: (1) Application of the meta-modeling concept to SRT, (2) Developing a *joint* base-meta model along with a comparison to white- and black-box alternatives, (3) Generating *asymmetric* uncertainty bounds in DNNs, and (4) Proposing a new evaluation methodology for SRT.

## 2. Related Work

Classical statistics on time series offers an abundance of work dealing with uncertainty quantification (Papoulis & Saunders, 1989). Most notably in econometrics, a variety of heteroskedastic variance models lead to highly successful application in financial market volatility analyses (Engle, 1982; Bollerslev, 1986; Mills, 1991). An Autoregressive Conditional Heteroskedastic, or ARCH, model (Engle, 1982), and its generalized version, GARCH, (Bollerslev, 1986) are two such methods, the latter of which serves as one of our baselines. They assume an autoregressive moving-average, or ARMA, model to underlie the variance series. Besides its stationarity assumptions, long horizon forecasting using (G)ARCH is difficult (Starica et al., 2005; Chen & Politis, 2019) and is typically used in a one-step-ahead setting. We use the GARCH as one of our baselines.

An illuminating study (Kendall & Gal, 2017) describes an integration of two sources of uncertainty, namely the *epistemic* (due to model) and the *aleatoric* (due to data). The authors propose a variational approximation of Bayesian Neural Networks and an implicit Gaussian model to quantify both types of variability in a non-sequential classifica-

tion and regression task. Based on (Nix & Weigend, 1994), (Lakshminarayanan et al., 2017a) also uses an implicit Gaussian model to improve the predictive performance of a base model, again in a non-sequential setting. Similar to (Kendall & Gal, 2017), the study does not focus on comparing the quality of the uncertainty to one generated by other methods. We adopt the implicit variance model of (Kendall & Gal, 2017; Oh et al., 2020; Lakshminarayanan et al., 2017a), as well as the method of variational dropout of (Gal & Ghahramani, 2016; Kendall & Gal, 2017) as baselines in our work. A meta-modeling approach was taken in (Chen et al., 2019) aiming at the task of instance filtering using white-box models. The work relates to ours through the meta-modeling concept but concentrates on classification in a non-sequential setting.

Besides its application in filtering, meta-modeling has been widely applied in the task of learning to learn and lifelong learning (Schmidhuber, 1987; Finn et al., 2019). However, it should be pointed out that the two applications of meta-modeling are not comparable due to their different objectives.

Uncertainty in data drift conditions was assessed in a recent study (Snoek et al., 2019). The authors employ calibration-based metrics to examine various methods for uncertainty in classification tasks (image and text data), and conclude, among others that most methods’ quality degrades with drift. Acknowledging drift as an important experimental aspect, our study takes it into account by testing in matched and drifted scenarios. Finally, (Shen et al., 2018) described a multi-objective training of a DNN in wind power prediction, minimizing two types of cost related to coverage and bandwidth. We expand on these metrics in Section 3.3.

## 3. Method

### 3.1. Meta Modeling Approach

The basic concept of Meta Modeling (MM), depicted in Figure 1, involves a combination of two models comprising a *base model*, performing the main task (e.g., regression), and a *meta model*, learning to predict the base model’s error behavior. Depending on the amount of information shared between these two, we distinguish several settings, namely (1) base model is a black-box (BB), (2) base is a white-box (WB, base parameters are accessible), and (3) base and meta components are trained jointly (JM). The advantages of WB and JM are obvious: rich information is available for the meta model to capture salient patterns for it to generate accurate predictions. On the other hand, the BB setting often occurs in practice and is a given.

We now formalize the MM concept as it applies to sequential regression. Let  $\hat{\mathbf{y}} = F_\phi(\mathbf{x})$  be the base model function parametrized by  $\phi$ , where  $\mathbf{x} = x_1, \dots, x_N$  and

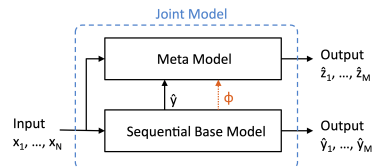


Figure 1. The concept of meta modeling

$\hat{\mathbf{y}} = \hat{y}_1, \dots, \hat{y}_M$  represent sequences of  $N$  input feature vectors and  $M$   $D$ -dimensional output vectors, with  $\hat{\mathbf{y}} \in \mathbb{R}^{D \times M}$ . Let  $\hat{\mathbf{z}} = G_\gamma(\hat{\mathbf{y}}, \mathbf{x}, \phi)$  denote the meta model, parameterized by  $\gamma$ , taking as input the predictions, the original features, and the parameters of the base to produce a sequence of error predictions,  $\hat{\mathbf{z}} \in \mathbb{R}^{D \times M}$ . The parameters  $\phi$  are obtained by solving an optimization problem,  $\arg \min_\phi \mathbb{E}[l_b(\hat{\mathbf{y}}, \mathbf{y})]$ , using a smooth loss function  $l_b$ , e.g., the Frobenius norm  $l_b = \|\hat{\mathbf{y}} - \mathbf{y}\|_F^2$ . Similarly, the parameters  $\gamma$  are determined via  $\arg \min_\gamma \mathbb{E}[l_m(\hat{\mathbf{z}}, \mathbf{z})] = \arg \min_\gamma \mathbb{E}[l_m(\hat{\mathbf{z}}, l_z(\hat{\mathbf{y}}, \mathbf{y}))]$  involving a loss  $l_z$  quantifying the target error (residual) from the base model, and  $l_m$  quantifying the prediction error of the meta model. In general,  $l_b$ ,  $l_z$ , and  $l_m$ , may differ<sup>1</sup>. The expectations are estimated using an available dataset. We used the  $L_F^2$  norm for  $l_b$  and  $l_m$ , and  $L_1$  for  $l_z$ , as described in Section 4. Given differentiable loss functions and the DNN setting, the base and the meta model can be integrated in a single network (JM). In this case the parameters are estimated jointly via

$$\phi^*, \gamma^* = \arg \min_{\phi, \gamma} \mathbb{E}[\beta l_b(\hat{\mathbf{y}}, \mathbf{y}) + (1 - \beta) l_m(\hat{\mathbf{z}}, l_z(\hat{\mathbf{y}}, \mathbf{y}))] \quad (1)$$

whereby dedicated output nodes of the network generate  $\hat{y}_t$  and  $\hat{z}_t$ , and  $\beta$  is a hyper-parameter trading off the base with the meta loss. Thus, one part of the network tackles the base task, minimizing the base residual, while another models the residual as the eventual measure of uncertainty. As done in (Kendall & Gal, 2017), one can argue that the base objective minimizes the epistemic (parametric) uncertainty, while the meta objective captures the aleatoric uncertainty present in the data. Due to their interaction, the base loss is influenced by the estimated uncertainty encouraging it to focus on feature-space regions with lower aleatoric uncertainty. Moreover, we conjecture, the DNN base model is encouraged to encode the input in ways suitable for uncertainty quantification.

Figure 2 shows an overview of a sequential DNN architecture applied throughout our study. It includes a base encoder-decoder pair and a meta decoder connected to them. Each of these contains a recurrent memory cell - the LSTM

<sup>1</sup>In classification, detection, and ranking tasks,  $l_b$  is typically a smooth surrogate for non-differentiable metrics, such as an error rate, or a ranking loss. In the BB and the WB setting the loss  $l_z$  may correspond to such metrics as differentiability is not required.

(Hochreiter & Schmidhuber, 1997). The role of the encoder is to process the sequential input,  $\mathbf{x}$ , compress its information in a context vector and pass it to the base decoder. The recurrent decoder produces the regression output  $\hat{\mathbf{y}}$  in  $M$  time steps feeding its predictions as input in the next time steps. Evolving in time, both base LSTMs update their internal states  $b_t$  and  $h_t$ , whereby the last state,  $b_N$ , serves as the context vector for the decoder. This architecture has gained wide popularity in applications such as speech-to-text (Chiu et al., 2018; Tüske et al., 2019), text-to-speech (Sotelo et al., 2017), machine translation (Sutskever et al., 2014), and image captioning (Rennie et al., 2016). Following the MM concept, we attach an additional decoder (the meta decoder) via connections to the encoder and decoder outputs. The context vector,  $b_N$ , is transformed by a fully connected layer (FCN in Figure 2), and both the  $\hat{y}_t$  output as well as the internal state,  $h_t$ , are fed into the meta component. As mentioned above, the meta decoder generates uncertainty estimates,  $\hat{z}_t$ .

Given the architecture depicted in Figure 2, we summarize the three settings as follows: (1) Joint Model (JM): parameters are trained according to Eq. (1) with certain values of  $\beta$ . (2) White-Box model (WB): base parameters  $\phi$  are trained first, followed by parameters  $\gamma$ , also accessing  $\phi$ . (3) Black-Box model (BB): same as (2) without access to  $\phi$ .

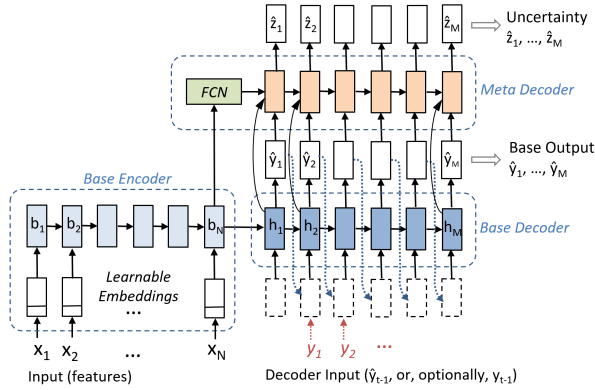


Figure 2. Encoder-Decoder architecture integrating a base and a meta model

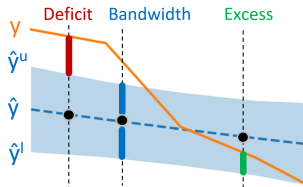


Figure 3. Bandwidth, excess, and deficit costs.

**Generating Symmetric and Asymmetric Bounds** The choice of loss function,  $l_z$ , gives rise to two scenarios. If  $l_z$  is an even function, e.g.,  $l_z(\hat{\mathbf{y}}, \mathbf{y}) = \|\hat{\mathbf{y}} - \mathbf{y}\|_1$ , the meta-

model targets  $\mathbf{z}$  capture base error equally in both directions: above and below the target. Hence, the uncertainty  $\hat{\mathbf{z}}$  predicted at test time will represent an interval symmetric around  $\hat{\mathbf{y}}$ . If, on the other hand,  $l_z$  takes the sign in  $z$  into account, it is possible to dedicate separate network nodes  $\gamma_l, \gamma_u \in \gamma$  to capturing lower and upper band estimates,  $\hat{\mathbf{z}}_l$  and  $\hat{\mathbf{z}}_u$ , respectively, thus accomplishing asymmetric prediction. Let  $\delta = \hat{\mathbf{y}} - \mathbf{y}$ . For the asymmetric scenario the meta objective is modified as follows:

$$\gamma^* = \arg \min_{\gamma} \mathbb{E}[l_m(\mathbf{z}_l, \max\{\delta, 0\}) + l_m(\mathbf{z}_u, \max\{-\delta, 0\})] \quad (2)$$

As with the popular Rectified Linear Units (Glorot et al., 2011), the non-differentiable points in Eq. (2) do not represent a practical problem for gradient descent optimizers.

Overall, for a  $D$ -dimensional regression output at time  $t$ ,  $y_t \in \mathbb{R}^D$ , the meta decoder will have  $D$  uncertainty output nodes in the symmetric and  $2D$  outputs in the asymmetric case.

### 3.2. Baselines

**Implicit Heteroskedastic Variance** (Lakshminarayanan et al., 2017a; Kendall & Gal, 2017; Oh et al., 2020) applied a Gaussian model  $\mathcal{N}(\mu, \sigma^2)$  to the output of a neural network predictor, where  $\mu$  represents the prediction and  $\sigma^2$  its uncertainty due to observational (aleatoric) noise. The model is trained to minimize the negative log-likelihood (NLL), with the variance being an implicit uncertainty parameter (in that it is trained indirectly) which is allowed to vary across the feature space (heteroskedasticity). We apply the Gaussian in the sequential setting by planting it onto the base decoder’s output (replacing the meta decoder) and train the network using the NLL objective:  $\phi^* = \arg \min_{\phi} \mathbb{E} \left[ \sum_{t=1}^M \sum_{d=1}^D \frac{(\hat{y}_{t,d} - y_{t,d})^2}{\sigma_{t,d}^2} + \log \sigma_{t,d}^2 \right]$  with  $D$  output nodes modeling the regression variable,  $\hat{y}_t$ , and separate  $D$  output nodes modeling the  $\log \sigma_t^2$ , at time  $t$ .

This approach resembles the meta-modeling concept somewhat but deviates in that the variance parameter is not supervised using the residual target but emerges as a by-product of the Gaussian model.

**Deep Ensembles** Ensembling of multiple NN models has been introduced in (Hansen & Salamon, 1990) to improve the prediction accuracy. Later, (Lakshminarayanan et al., 2017b) utilized ensembles for uncertainty quantification and showed them to be an effective alternative to Bayesian NNs. Deep ensembles have quickly become a widely-used baseline (Snoek et al., 2019; Gustafsson et al., 2019).

In this work, we include ensembling as another baseline. Multiple copies of the base model (i.e., the network without the meta decoder component shown in Figure 2) are trained

using random initialization. At test time, the resulting models produce multiple sequential predictions whose mean and variance serve as the target and the uncertainty predictions, respectively. As each training run results a different local-optimum model the ensemble represents a sampling of the parameter space thus capturing the parametric (epistemic) uncertainty (in contrast to the implicit variance and the meta-model).

**Variational Dropout** (Gal & Ghahramani, 2016) established a connection between dropout (Srivastava et al., 2014), i.e., the process of randomly omitting network connections, and an approximate Bayesian inference. Their work suggests applying the dropout principle to the inputs, internal states, as well as outputs of the recurrent cells. However, unlike with traditional dropout, the method is applied both in training and test, and for each RNN sequence the dropout pattern is kept fixed. We apply the variational dropout method to the base encoder and decoder. By performing multiple runs per test sequence, each with a different random dropout pattern, the base predictions are calculated as the mean and the base uncertainty as the variance over such runs. Similar to ensembling, this variational approximation of the Bayesian method captures the parametric (epistemic) uncertainty of the model.

**GARCH Variance** Introduced in (Bollerslev, 1986; Engle, 1982), the Generalized Autoregressive Conditional Heteroskedastic (GARCH) variance model belongs among the most popular statistical methods. A GARCH(p,q) assumes the series to follow an autoregressive moving average model and estimates the variance at time  $t$  as a linear combination of past  $q$  residual terms,  $\epsilon^2$ , and  $p$  previous variances,  $\sigma^2$ :  $\sigma_t^2 = \alpha_0 + \sum_{i=1}^q \alpha_i \epsilon_{t-i}^2 + \sum_{i=0}^p \beta_i \sigma_{t-i}^2$ .

The  $\alpha_0$  term represents a constant component of the variance. The parameters,  $\alpha, \beta$  are estimated via maximum-likelihood on a training set. The GARCH process relates to the concept in Figure 1 in that it acts as the meta-model predicting the squared residual. At training time, we take the residual  $\epsilon_t = \hat{y}_t - y_t$  using predictions from the base model, while at test time, the residual is approximated using an autoregressive component. We use the GARCH as a baseline only on one of the datasets for reasons discussed in Section 4.

**Constant-Band Baseline** A consistent comparison of uncertainty methods is difficult due to the fact that each generates an uncertainty around different base predictions. Therefore, as a reference we also generate a constant symmetric band around each base predictor. Such a bound represents a homoskedastic process – a sensible choice in many well-behaved sequential regression problems, corresponding to a GARCH(0,0) model. We will use this reference point

to compute a relative gain of each method as explained in Section 3.3.

### 3.3. Evaluation Methodology

**Core Metrics** Unlike with classification tasks, where standard calibration-based metrics apply (Snoek et al., 2019), we need to consider two aspects arising in regression, roughly speaking: (1) what is the extent of observations falling outside the uncertainty bounds (Type 1 cost), and (2) how excessive are the bounds (Type 2 cost). An optimal bound captures all of the observation while being least excessive in terms of its bandwidth. (Shen et al., 2018), among others, defined two measures reflecting these aspects (miss rate and bandwidth) which we adopt below (Eqs. (3) and (4)) while adding two refinements (Eqs. (5) and (6)). Let  $\hat{y}^l = \hat{y} - \hat{z}_l$  and  $\hat{y}^u = \hat{y} + \hat{z}_u$  denote the predicted lower and upper bound, respectively. Recall that  $\hat{y} \in \mathbb{R}^{D \times M}$ . We define the following metrics:

$$\text{Missrate}(\hat{y}^l, \hat{y}^u, \mathbf{y}) = 1 - \frac{1}{MD} \sum_{d,t: y_{dt} \in [\hat{y}_{dt}^l, \hat{y}_{dt}^u]} 1 \quad (3)$$

$$\text{Bandwidth}(\hat{y}^l, \hat{y}^u, \mathbf{y}) = \frac{1}{2MD} \sum_{d=1}^D \sum_{t=1}^M \hat{y}_{dt}^u - \hat{y}_{dt}^l \quad (4)$$

$$\begin{aligned} \text{Excess}(\hat{y}^l, \hat{y}^u, \mathbf{y}) &= \\ &= \frac{1}{MD} \sum_{d,t: y_{dt} \in [\hat{y}_{dt}^l, \hat{y}_{dt}^u]} \min \{ y_{dt} - \hat{y}_{dt}^l, \hat{y}_{dt}^u - y_{dt} \} \end{aligned} \quad (5)$$

$$\begin{aligned} \text{Deficit}(\hat{y}^l, \hat{y}^u, \mathbf{y}) &= \\ &= \frac{1}{MD} \sum_{d,t: y_{dt} \notin [\hat{y}_{dt}^l, \hat{y}_{dt}^u]} \min \{ |y_{dt} - \hat{y}_{dt}^l|, |y_{dt} - \hat{y}_{dt}^u| \} \end{aligned} \quad (6)$$

Figure 3 illustrates these metrics. The relative proportion of observations lying outside the bounds (miss rate) ignores the *extent* of the bound’s short fall. The Deficit, Eq. (6), captures this. The type 2 cost is captured by the Bandwidth, Eq. (4). However, its range is indirectly compounded by the underlying variation in  $\hat{y}$  and  $\mathbf{y}$ . Therefore we propose the Excess measure, Eq. (5), which also reflects the Type 2 cost, but just the portion above the minimum bandwidth necessary to include the observation.

Finally, for symmetric bounds, we also record the correlation,  $\rho$ , between the absolute difference  $|\delta| = |\hat{y} - \mathbf{y}|$  and the (one-sided) uncertainty band  $\hat{z}$ . Intuitively, a good-quality prediction interval will correlate well with the amplitude

$|\delta|$ , and vice versa. In the experimental results, we report as  $\rho$  the average of the Pearson and the Spearman correlation coefficients.

**Calibration** In general, DNNs offer few guarantees about the behavior of their output. DNNs tend to produce miscalibrated classification probabilities (Guo et al., 2017). In order to evaluate the uncertainty across models, it is necessary to establish a common operating point (OP). We achieve this via a scaling calibration. For symmetric bounds, we assume that  $\mathbf{y} = \hat{\mathbf{y}} + \hat{\mathbf{z}} \odot \epsilon$  where  $\epsilon \in \mathbb{R}^{D \times M}$  is a random i.i.d. matrix and  $\hat{\mathbf{z}}$  is the predicted non-negative uncertainty band. Let  $Z_{dt} = \frac{y_{dt} - \hat{y}_{dt}}{\hat{z}_{dt}}$ . Using a held-out dataset, we can obtain an empirical distribution in each output dimension:  $\text{cdf}(\{Z_{dt}\}_{1 \leq t \leq M})$ ,  $d = 1, \dots, D$ . It is then possible to find the value  $\varepsilon_d^{(p)}$  for a desired quantile  $p$ , e.g.,  $\varepsilon_d^{(0.95)}$ , and construct the prediction bound at test time:  $[\hat{y}_{dt} - \hat{z}_{dt}\varepsilon_d^{(p)}, \hat{y}_{dt} + \hat{z}_{dt}\varepsilon_d^{(p)}]$ . Assuming  $Z_d$  is stationary, in expectation, this bound will contain the desired proportion  $p$  of the observations, i.e.,  $\mathbb{E}[\text{Missrate}(\hat{\mathbf{y}}^t, \hat{\mathbf{y}}^u, \mathbf{y})] = 1 - p$ .

This scaling is applied in our evaluation to compare the excess, bandwidth and deficit at fixed miss rates as well as setting a minimum cost OP (see Section 3.3). An Algorithm to find a scale factor for a desired value of any of the four metrics in  $O(M^2)$  operations is given in the Appendix.

**Metrics Used in Reporting** Recall that an OP refers to a value of a desired metric measured at a fixed value of a second metric. The following OP-based measures are used in reporting: (1) Excess, Deficit, Bandwidth at a fixed Missrate, averaged over  $\text{Missrate} = \{0.1, 0.05, 0.01\}$ , and (2) Minimum Excess-Deficit cost, where  $\text{cost} = \frac{1}{2}(\text{Excess} + \text{Deficit})$  with the minimum found over all calibrations (OPs).

For each system and measure,  $m_s$ , a symmetric constant-band baseline,  $m_{fixed}$ , is also generated and a relative gain with respect to this reference calculated:  $gain_s = 100 \times \frac{m_{fixed} - m_s}{m_{fixed}} \%$ . Finally, the error rate of the base predictor is calculated as  $E_{base}(\hat{\mathbf{y}}, \mathbf{y}) = \frac{1}{D} \sum_{d=1}^D \frac{\|\hat{y}_d - y_d\|_1}{\|y_d\|_1}$ , where  $\hat{y}_d, y_d$  are  $d$ -th row vectors of  $\hat{\mathbf{y}}, \mathbf{y}$ .

## 4. Experiments

**Datasets** Two sequential regression datasets, namely the *Metro Interstate Traffic Volume (MITV)* dataset<sup>2</sup> and the *SPE9 Reservoir Production Rates (SPE9PR)* dataset<sup>3</sup>, were experimented with. Both originate from real-world applications, involve sequential input/output variables, and provide

<sup>2</sup><https://archive.ics.uci.edu/ml/machine-learning-databases/00492/>

<sup>3</sup><https://developer.ibm.com/technologies/artificial-intelligence/data/oil-reservoir-simulations>

for scenarios with varying degrees of difficulty.

The MITV dataset is a collection of hourly weather features with the target of the regression being the hourly traffic volume, recorded by the Minnesota DoT continuously between 2012 and 2018. The SPE9PR, on the other hand, is a large collection of mathematical simulations of a reservoir field with varying input and output sequences with each simulation comprising a sequence with 100 time steps. The regression targets in this case are multivariate and correspond to field production rates. The SPE9PR also contains a data partition collected under distributional drift. Full detail on both datasets including their preprocessing can be found in the Appendix.

In general, there is a notable scarcity of publicly available datasets with the characteristics needed for this study, namely: (1) providing sufficient amounts of data to train and evaluate DNNs, (2) being sequential, and (3) being a regression task. The two datasets in this study satisfy these criteria and represent diverse, practical real-world applications.

**Training Procedure** Each dataset was partitioned into TRAIN, DEV, DEV2, and TEST sets (with SPE9PR also providing a TEST-drift set), as listed Table 1. While the TRAIN/DEV partitions served basic training, the DEV2 was used in determining hyperparameters and operating points (calibration). The TEST sets were used to produce the reported metrics. While a single sample in the SPE9PR represents a complete sequence of 100 steps, the MITV data come as a single contiguous sequence. The partitioning of the MITV set is strictly ordered by time, whereby the DEV sequence follows TRAIN, DEV2 follows DEV, and TEST follows DEV2. After partitioning, each MITV sequence was processed by a sliding window of length 36 hours (in 1-hour steps). This resulted in a series of  $(n - 35) \times 36$  subsequences ( $n$  denotes the partition size) to feed the encoder-decoder model. When testing on the MITV, DNN predictions from such sliding windows were recombined into a contiguous prediction sequence again.

The base encoder-decoder network (see Figure 2) is trained using the Adam optimizer (Kingma & Ba, 2014) with a varying initial learning rate, lr, in two stages: (1) Training of all parameters using TRAIN while providing the ground truth as the decoder input at each time step. (2) Building on the previous, the training continues, however, decoder predictions from step  $t - 1$  are fed as decoder inputs at step  $t$ —a mode referred to as *emulation* by (Bengio et al., 2015).

All DNN models were implemented in Tensorflow 1.11. We used the `arch` package in Python as implementation of the GARCH model. Additional details on implementation as well as all hyperparameters are given in the Appendix.

Table 1. Overview statistics of the MITV and the SPE9PR datasets

Dataset	Total Samples	Input Features	Output Dim	Time Resol.	Partition Size			
					TRAIN	DEV	DEV2	TEST
MITV	48204	8	1	1 hr	33744	4820	4820	4820
SPE9PR	28000 ×100	248	4	90 days	24000 ×100	1000 ×100	1000 ×100	1000 ×100

**Joint Model, Symmetric (JMS), and Asymmetric (JMA):** The common training steps are performed using the objective in Eq. (1), with  $\beta = 1.0$ , first. Then, the joint training continues with  $\beta = 0.5$  as long as the objective improves on DEV. In a final step, the model switches to using DEV as training with  $\beta = 0.0$  until no improvement on TRAIN is seen. A similar procedure is followed for the JMA, except using Eq. (2).

**White-Box Model, Symmetric (WBMS):** The basic training is performed with  $\beta = 1.0$ . Next, only meta model parameters are estimated using the DEV/TRAIN sets with  $\beta = 0.0$ .

**Black-Box Model, Symmetric (BBMS):** Base training is performed. The base model processes the DEV set to generate residual  $\mathbf{z}$ . A separate encoder-decoder model is then trained using  $(\mathbf{x}, \mathbf{z})$ .

**Joint Model with Variance (JMV):** The two common steps are performed using the NLL objective (see Section 3.2) with the variance-related parameters first fixed, and, in a subsequent step, allowing the variance parameters to be adjusted, until convergence. This is to aid stability in training (Nix & Weigend, 1994). To obtain a more precise comparison with the JMS/JMA training procedure we alternatively adjust only the variance parameter (an analogy to the case of  $\beta = 0.0$  with JMS) in a final step using the DEV partition.

**Ensemble (ENSMB):** A total of 10 separate models with random initialization are trained according the stage (1) and (2) as outlined above. At test time, the 10 models are run on each test sequence to obtain the mean prediction and standard deviation.

**Dropout Model Symmetric (DOMS):** Dropout with a rate of 0.25 (inputs, outputs) and 0.1 (internal states), determined as best performing on the DEV2 set, were applied in both the base encoder and the decoder. The two common steps were performed. At test time, the model was run 10 times per each test sequence to obtain the mean prediction and standard deviation.

**GARCH:** The GARCH model from Section 3.2 is used with  $p = q = 5$ . The lag value was determined using an autocorrelation chart showing attenuation at lags  $> 5$ . We only apply this baseline to the MITV dataset as it provides a contiguous time series. The model parameters were trained using the DEV2 partition.

Throughout the experiments, the size of each LSTM cell was kept fixed at 32 for the base encoder/decoder, and at 16 for the meta decoder. The base sizing has been largely driven by our preliminary study showing it suffices in providing accurate base predictions.

**Testing Procedure** As mentioned above the SPE9PR dataset has two TEST partitions: one for a matched and one for a drifted condition. While the MITV dataset does not provide an explicit source of drift, we induce drift by creating a discrepancy in the modeling procedure between training and test: In the non-drift condition, the DNN’s decoder is given access to the past 12 hours worth of traffic observations to make a forecast for the next 24 hours. This is achieved by spanning a 36-hour window and feeding the decoder inputs the first 12 hours of ground truth, during training. Now to create the drift scenario we test the MITV model without providing those first 12 hours of observations and the model uses their own predictions for that period instead. This emulates a “model drift” condition in that the model, trained to rely on actual observations, is getting its own noisy predictions.

**Results with Symmetric Bounds** Table 2 compares the proposed symmetric-bounds systems (JMS, WBMS, BBMS) with the baselines (JMV, ENSMB, DOMS, GARCH). The relative error of the base predictor is given in the  $E_{base}$  column. The uncertainty quality reported in Table 2 is the average gain in excess-deficit metrics, as defined in Section 3.3. Columns labeled as  $G^*$  contain measurements made at an operating point (OP) determined on the test set itself, while those labeled as  $G^x$  use an OP from a held-out (DEV2) set. While  $G^x$  reflects generalization of the calibration,  $G^*$  values are interesting as they reveal the potential of each method. Furthermore, in the  $\rho$  column we give the correlation metric defined in Section 3.3. Based on a paired permutation test (Dwass, 1957) all but entries marked with † are mutually significant at  $p < 0.01$ .

From Table 2 we make the following observations: (1) the JMS model dominates all other models across all conditions. The fact that it outperforms the WBMS indicates there is a benefit to the joint training setup, as conjectured earlier. (2) The WBMS dramatically outperforms the BBMS model, which remains only as good as a constant band for

MITV data, indicating it is hard to reliably predict residuals from only the input features. (3) The most competitive baseline is the JMV model. As discussed in Section 3.2, the JMV shares some similarity with the meta-modeling approach. (4) The JMS and WBMS models perform particularly well in the strong drift scenario (SPE9PR), suggesting that white-box features play an essential role in achieving generalization. (5) the DOMS and ENSMB baselines work well with ENSMB outperforming DOMS in most conditions. On SPE9PR, the DOMS model provides largely no benefit. In almost all cases, the averaging of base predictions in both DOMS and ENSMB results in lowest error rates of the base predictor. Finally, (6) with a few exceptions, the  $\rho$  measure appears to be a good indicator of the overall ranking, aligning with the gain metrics reported.

We want to point out that the meta-model training uses the DEV partition for tuning the meta-model parameters in a final step (see Section 4). In this context, a question arises whether a similar tuning step could help the JMV model’s variance parameter. We followed the alternative training steps described in Section 4 and updated the variance-related network nodes while keeping the rest of the network fixed. By comparing these two variants we conclude that this additional tuning step does not benefit the JMV model. A table with complete results and a discussion can be found in the Appendix.

Representative samples of JMS and JMV uncertainty bounds are shown in Figure 4 (MITV) and Figure 5 (SPE9PR). They illustrate a clear trend we observed in the tests, namely that the JMS (also seen with WBMS) model are better able to cover the actual observation, particularly when the base prediction tends to make large errors. By visual assessment, the joint model (JMS) shows a striking capability to account for uncertainty patterns, especially in the SPE9PR drift conditions. These examples are not isolated. Indeed it appears that the sequential nature of the joint meta model is able to learn such patterns with a significantly higher precision, as reflected in the summary metrics as well. Additional plots can be found in the Appendix, and *all test samples* can be visualized in a notebook provided as part of the Supplementary Material.

**Results with Asymmetric Bounds** Generating asymmetric bounds is a new intriguing aspect of DNN-based meta-models. Using the JMA model, we first recorded the accuracy with which the asymmetric output agrees *in sign* (orientation) with the observed base discrepancy. Averaged over each of the two datasets, this accuracy is at 83.3%, and 91.1%. The promise of asymmetric bounds lies in its potential to reduce the *bandwidth* cost. Since the Excess and Deficit metrics ignore the absolute bandwidth, we also evaluate the JMA model using the Bandwidth metric (Eq. (4)), averaged over the same OPs. The results are shown in Table

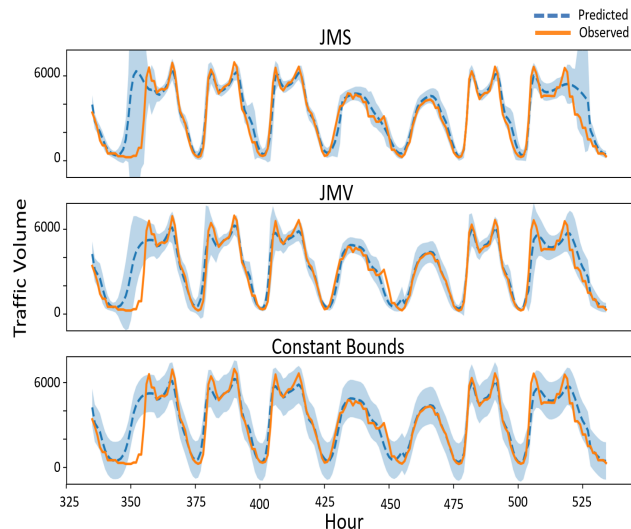


Figure 4. Sample of traffic volume predictions with uncertainty generated by the JMS and JMV models, along with a constant bound (around JMV) (miss rate set to 0.1 on TEST).

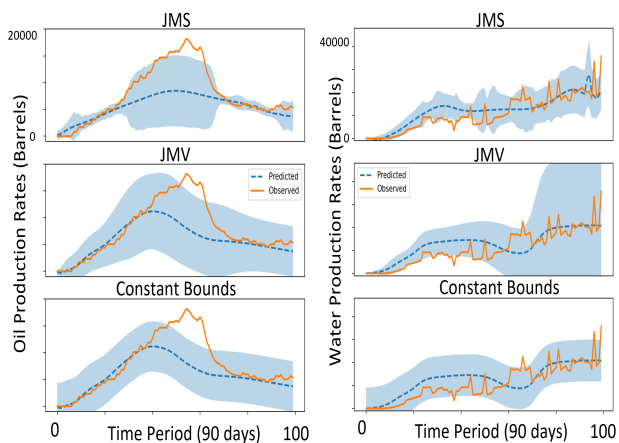


Figure 5. SPE9PR samples of oil (left) and water (right) production rates (“drift” scenario, miss rate set to 0.1 on TEST).

Table 2. Relative optimum ( $G^*$ ) and cross-validated gains ( $G^x$ ) using the Excess-Deficit metrics.  $\rho$  is the correlation defined in Section 3.3.  $E_{base}$  denotes the base predictor’s error. Within each column, elements marked<sup>†</sup> are in a statistical tie, all other values are mutually significant at  $p < 0.01$

System	MITV								SPE9PR							
	Match				Model Drift				Match				Data Drift			
	$E_{base}$	$\%G^*$	$\%G^x$	$\rho$	$E_{base}$	$\%G^*$	$\%G^x$	$\rho$	$E_{base}$	$\%G^*$	$\%G^x$	$\rho$	$E_{base}$	$\%G^*$	$\%G^x$	$\rho$
JMS	.155 <sup>†</sup>	<b>57.8<sup>†</sup></b>	<b>59.3<sup>†</sup></b>	<b>.721<sup>†</sup></b>	.187 <sup>†</sup>	<b>52.5</b>	<b>55.6</b>	<b>.721</b>	.165	<b>46.5</b>	<b>46.6</b>	.637	.291	<b>56.6</b>	<b>50.5</b>	<b>.726<sup>†</sup></b>
WBMS	.159 <sup>†</sup>	<b>53.8<sup>†</sup></b>	<b>55.3<sup>†</sup></b>	<b>.704<sup>†</sup></b>	.190 <sup>†</sup>	39.4	42.3	.637	.162	44.8	44.9	.659	.313	54.5	43.8	<b>.731<sup>†</sup></b>
JMV	.167	20.4	25.5	.546	.179	20.0 <sup>†</sup>	17.5 <sup>†</sup>	.500	.159	45.3	45.5	.586	.334	-6.5	4.4	.391
ENSMB	.133	14.8	17.1	.464	.164	10.4	6.1	.502	.160	21.2	20.3	.434	.343	5.9	-33.1	.416
DOMS	.144	13.2	12.8	.278	.155	16.6 <sup>†</sup>	17.3 <sup>†</sup>	.380	.177	1.3	1.4	.154	.279	-0.2	-5.2	.075
BBMS	.153 <sup>†</sup>	-0.4	1.2	.161	.188 <sup>†</sup>	-8.9	-3.0	.102	.170	31.9	30.3	.408	.326	11.6	12.8	.325
GARCH	.155 <sup>†</sup>	-1.8	3.1	.134	.187 <sup>†</sup>	-14.7	-4.0	-.033	n/a	n/a	n/a	n/a	n/a	n/a	n/a	n/a

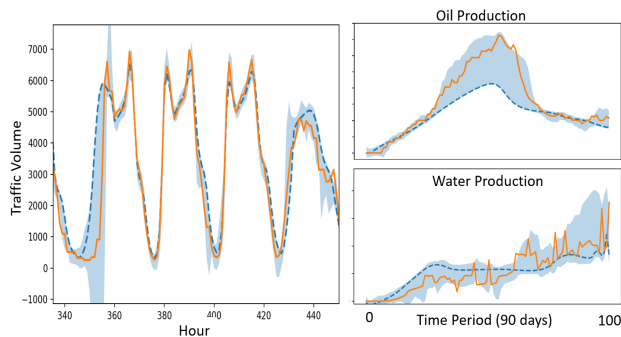


Figure 6. Samples of asymmetric bounds produced by the JMA. MITV sample (left) and SPE9PR (right) correspond to segments shown in Figure 4 and 5.

3 comparing the JMA model to the best symmetric model, JMS. The JMS model outperforms JMA in all scenarios on Excess-Deficit, however, compared on the bandwidth metric, the JMA dominates benefiting from its orientation capability. Upon visual inspection the output of the JMA is appreciably better in bandwidth: Figure 6 shows samples on both datasets. In most instances the bounds behave as expected, expending the bulk of bandwidth in the correct direction.

An interesting question arises whether it is possible to utilize the asymmetric output as a correction to the base predictor. Our preliminary investigation shows that a naive combination leads to degradation in the base error, however, this question remains of interest for future work.

## 5. Conclusions

In this work we demonstrated that meta-modeling (MM) provides a powerful new framework for uncertainty prediction. Through a systematic evaluation of the proposed MM variants we report considerable relative gains over a

Table 3. Relative optimum (opt.) and cross-validated (xval) gains on Bandwidth and Excess-Deficit metrics for the asymmetric JMA model.

Evaluation	MITV		SPE9PR		
	match	drift	match	drift	
JMA Base Error	.158	.200	.168	.320	
Bandwidth	JMA, opt. % gain	<b>44.1</b>	<b>37.0</b>	<b>35.5</b>	<b>54.3</b>
	JMA, xval % gain	33.1	26.4	35.5	8.5
	JMS, opt. % gain	37.5	31.6	29.1	34.3
	JMS, xval % gain	35.2	27.2	28.7	-4.4
Ex-Deficit	JMA, opt. % gain	45.3	29.0	30.9	50.8
	JMA, xval % gain	40.4	28.6	30.8	24.2
	JMS, opt. % gain	57.8	52.5	<b>46.5</b>	<b>56.6</b>
	JMS, xval % gain	<b>59.3</b>	<b>55.6</b>	46.6	50.5

constant-band reference and demonstrate that they outperform all competitive baselines while showing stability across drift scenarios. A jointly trained model integrating the base with a meta component fares best, followed by a white-box setup, indicating that trainable white-box features play an essential role in the task. Besides symmetric uncertainty, we also investigated generating asymmetric bounds using dedicated network nodes and showed their benefit in reducing the uncertainty bandwidth. We believe these results open an exciting new research avenue for uncertainty quantification in sequential regression.

## References

- Arnold, M., Bellamy, R. K. E., Hind, M., Houde, S., Mehta, S., Mojsilović, A., Nair, R., Ramamurthy, K. N., Olteanu, A., Piorkowski, D., Reimer, D., Richards, J., Tsay, J., and Varshney, K. R. Factsheets: Increasing trust in ai services through supplier’s declarations of conformity. *IBM Journal of Research and Development*, 63(4/5):6:1–6:13, July 2019. ISSN 0018-8646. doi: 10.1147/JRD.2019.2942288.

- Begoli, E., Bhattacharya, T., and Kusnezov, D. The need for uncertainty quantification in machine-assisted medical decision making. *Nature Mach Intell*, 1:20–23, 2019.
- Bengio, S., Vinyals, O., Jaitly, N., and Shazeer, N. Scheduled sampling for sequence prediction with recurrent neural networks. In *Proceedings of the 28th International Conference on Neural Information Processing Systems - Volume 1*, NIPS’15, pp. 1171–1179, Cambridge, MA, USA, 2015. MIT Press.
- Bollerslev, T. Generalized autoregressive conditional heteroskedasticity. *Journal of Econometrics*, 31(3):307–327, April 1986.
- Chen, J. and Politis, D. N. Optimal multi-step-ahead prediction of arch/garch models and novas transformation. *Econometrics*, 7(3):34, Aug 2019. ISSN 2225-1146. doi: 10.3390/econometrics7030034.
- Chen, T., Navrátil, J., Iyengar, V., and Shanmugam, K. Confidence scoring using whitebox meta-models with linear classifier probes. In *The 22nd International Conference on Artificial Intelligence and Statistics, AISTATS 2019, 16-18 April 2019, Naha, Okinawa, Japan*, pp. 1467–1475, 2019.
- Chiu, C., Sainath, T. N., Wu, Y., Prabhavalkar, R., Nguyen, P., Chen, Z., Kannan, A., Weiss, R. J., Rao, K., Gonnina, E., Jaitly, N., Li, B., Chorowski, J., and Bacchiani, M. State-of-the-art speech recognition with sequence-to-sequence models. In *2018 IEEE International Conference on Acoustics, Speech and Signal Processing (ICASSP)*, pp. 4774–4778, April 2018.
- Dwass, M. Modified randomization tests for nonparametric hypotheses. *Ann. Math. Statist.*, 28(1):181–187, 03 1957. doi: 10.1214/aoms/1177707045.
- Engle, R. F. Autoregressive conditional heteroscedasticity with estimates of the variance of united kingdom inflation. *Econometrica*, 50(4):987–1007, 1982. ISSN 00129682, 14680262.
- Finn, C., Rajeswaran, A., Kakade, S., and Levine, S. Online meta-learning. In Chaudhuri, K. and Salakhutdinov, R. (eds.), *Proceedings of the 36th International Conference on Machine Learning*, volume 97 of *Proceedings of Machine Learning Research*, pp. 1920–1930, Long Beach, California, USA, 09–15 Jun 2019. PMLR.
- Gal, Y. and Ghahramani, Z. A theoretically grounded application of dropout in recurrent neural networks. In Lee, D. D., Sugiyama, M., Luxburg, U. V., Guyon, I., and Garnett, R. (eds.), *Advances in Neural Information Processing Systems 29*, pp. 1019–1027. Curran Associates, Inc., 2016.
- Glorot, X., Bordes, A., and Bengio, Y. Deep sparse rectifier neural networks. In Gordon, G., Dunson, D., and Dudík, M. (eds.), *Proceedings of the Fourteenth International Conference on Artificial Intelligence and Statistics*, volume 15 of *Proceedings of Machine Learning Research*, pp. 315–323, Fort Lauderdale, FL, USA, 11–13 Apr 2011. PMLR.
- Guo, C., Pleiss, G., Sun, Y., and Weinberger, K. Q. On calibration of modern neural networks. In *Proceedings of the 34th International Conference on Machine Learning - Volume 70*, ICML’17, pp. 1321–1330. JMLR.org, 2017.
- Gustafsson, F. K., Danelljan, M., and Schön, T. B. Evaluating scalable bayesian deep learning methods for robust computer vision. *CoRR*, abs/1906.01620, 2019. URL <http://arxiv.org/abs/1906.01620>.
- Hansen, L. K. and Salamon, P. Neural network ensembles. 12(10):993–1001, October 1990. ISSN 0162-8828. doi: 10.1109/34.58871.
- Hochreiter, S. and Schmidhuber, J. Long short-term memory. *Neural Comput.*, 9(8):1735–1780, November 1997. ISSN 0899-7667. doi: 10.1162/neco.1997.9.8.1735.
- Jiang, H., Kim, B., Guan, M., and Gupta, M. To trust or not to trust a classifier. In Bengio, S., Wallach, H., Larochelle, H., Grauman, K., Cesa-Bianchi, N., and Garnett, R. (eds.), *Advances in Neural Information Processing Systems 31*, pp. 5541–5552. Curran Associates, Inc., 2018.
- Kendall, A. and Gal, Y. What uncertainties do we need in bayesian deep learning for computer vision? In Guyon, I., Luxburg, U. V., Bengio, S., Wallach, H., Fergus, R., Vishwanathan, S., and Garnett, R. (eds.), *Advances in Neural Information Processing Systems 30*, pp. 5574–5584. Curran Associates, Inc., 2017.
- Killough, J. Ninth SPE comparative solution project: A reexamination of black-oil simulation. In *SPE Reservoir Simulation Symposium*. Society of Petroleum Engineers, 1995. doi: 10.2118/29110-ms.
- Kingma, D. P. and Ba, J. Adam: A method for stochastic optimization, 2014. cite arxiv:1412.6980Comment: Published as a conference paper at the 3rd International Conference for Learning Representations, San Diego, 2015.
- Lakshminarayanan, B., Pritzel, A., and Blundell, C. Simple and scalable predictive uncertainty estimation using deep ensembles. In Guyon, I., Luxburg, U. V., Bengio, S., Wallach, H., Fergus, R., Vishwanathan, S., and Garnett, R. (eds.), *Advances in Neural Information Processing Systems 30*, pp. 6402–6413. Curran Associates, Inc., 2017a.

- Lakshminarayanan, B., Pritzel, A., and Blundell, C. Simple and scalable predictive uncertainty estimation using deep ensembles. In *NIPS*, 2017b.
- Madry, A., Makelov, A., Schmidt, L., Tsipras, D., and Vladu, A. Towards deep learning models resistant to adversarial attacks. *ArXiv*, abs/1706.06083, 2017.
- Mills, T. C. *Time Series Techniques for Economists*. Number 9780521405744 in Cambridge Books. Cambridge University Press, 1991.
- Nix, D. A. and Weigend, A. S. Estimating the mean and variance of the target probability distribution. In *Proceedings of 1994 IEEE International Conference on Neural Networks (ICNN'94)*, volume 1, pp. 55–60 vol.1, June 1994. doi: 10.1109/ICNN.1994.374138.
- Oh, M., Olsen, P. A., and Ramamurthy, K. N. Crowd counting with decomposed uncertainty. In *AAAI Conference on Artificial Intelligence*, 2020.
- Papoulis, A. and Saunders, H. Probability, Random Variables and Stochastic Processes (2nd Edition). *Journal of Vibration, Acoustics, Stress, and Reliability in Design*, 111(1):123–125, 01 1989. ISSN 0739-3717. doi: 10.1115/1.3269815.
- Rennie, S. J., Marcheret, E., Mroueh, Y., Ross, J., and Goel, V. Self-critical sequence training for image captioning. *CoRR*, abs/1612.00563, 2016.
- Schmidhuber, J. Evolutionary principles in self-referential learning. on learning now to learn: The meta-meta-meta...-hook. Diploma thesis, Technische Universität München, Germany, 14 May 1987. URL <http://www.idsia.ch/~juergen/diploma.html>.
- Shen, Y., Wang, X., and Chen, J. Wind power forecasting using multi-objective evolutionary algorithms for wavelet neural network-optimized prediction intervals. *Applied Sciences*, 8(2):185, Jan 2018. ISSN 2076-3417. doi: 10.3390/app8020185.
- Snoek, J., Ovadia, Y., Fertig, E., Lakshminarayanan, B., Nowozin, S., Sculley, D., Dillon, J., Ren, J., and Nado, Z. Can you trust your model’s uncertainty? evaluating predictive uncertainty under dataset shift. In *Advances in Neural Information Processing Systems*, pp. 13969–13980, 2019.
- Sotelo, J., Mehri, S., Kumar, K., Santos, J. F., Kastner, K., Courville, A. C., and Bengio, Y. Char2wav: End-to-end speech synthesis. In *5th International Conference on Learning Representations, ICLR 2017, Toulon, France, April 24-26, 2017, Workshop Track Proceedings*, 2017.
- Srivastava, N., Hinton, G., Krizhevsky, A., Sutskever, I., and Salakhutdinov, R. Dropout: A simple way to prevent neural networks from overfitting. *Journal of Machine Learning Research*, 15:1929–1958, 2014.
- Starica, C., Herzel, S., and Nord, T. Why does the GARCH(1,1) model fail to provide sensible longer-horizon volatility forecasts? Econometrics 0508003, University Library of Munich, Germany, August 2005.
- Sutskever, I., Vinyals, O., and Le, Q. V. Sequence to sequence learning with neural networks. In *Proceedings of the 27th International Conference on Neural Information Processing Systems - Volume 2, NIPS'14*, pp. 3104–3112, Cambridge, MA, USA, 2014. MIT Press.
- Tüske, Z., Audhkhasi, K., and Saon, G. Advancing sequence-to-sequence based speech recognition. *Proc. Interspeech 2019*, pp. 3780–3784, 2019.

---

**Algorithm 1** Find best scale for a given metric value
 

---

**Input:** Observation, base and meta predictions  $\{\hat{y}_t, y_t, \hat{z}_t^l, \hat{z}_t^u\}_{1 \leq t \leq M}$ ; metric function  $f$ ; target value  $\rho^*$

**Output:** Scale factor  $\varepsilon^*$

**for**  $t \leftarrow 1$  **to**  $M$  **do**

$\delta_t \leftarrow \hat{y}_t - y_t$ .

$\varepsilon_t \leftarrow \begin{cases} \frac{\delta_t}{\hat{z}_t^l} & \text{for } \delta_t \geq 0 \\ -\frac{\delta_t}{\hat{z}_t^u} & \text{otherwise} \end{cases}$

**for**  $k \leftarrow 1$  **to**  $M$  **do**

$\hat{y}_k^l \leftarrow \hat{y}_k - \varepsilon_t \hat{z}_k^l$

$\hat{y}_k^u \leftarrow \hat{y}_k - \varepsilon_t \hat{z}_k^u$

**end for**

$\rho_t \leftarrow f(\{\hat{y}_k^l, \hat{y}_k^u, y_k\}_{1 \leq k \leq M})$

**end for**

$t^* \leftarrow \arg \min_t |\rho_t - \rho^*|$

$\varepsilon^* \leftarrow \varepsilon_{t^*}$

---

## A. Algorithm to Find a Scaling Factor

Section 3.3 discusses the scaling calibration in the context of the four metrics: Missrate, Bandwidth, Excess, and Deficit. Algorithm 1 finds a scale factor for a desired value of any of these four metrics in  $O(M^2)$  operations.

## B. Additional Dataset and Implementation Details

### B.1. Datasets

#### B.1.1. METRO INTERSTATE TRAFFIC VOLUME (MITV)

The dataset is a collection of hourly westbound-traffic volume measurements on Interstate 94 reported by the Minnesota DoT ATR station 301 between the years 2012 and 2018. These measurements are aligned with hourly weather features<sup>4</sup> as well as holiday information, also part of the dataset. The target of regression is the hourly traffic volume. This dataset was released in May, 2019.

The MITV input features were preprocessed to convert all categorical features to trainable vector embeddings, as outlined in Figure 2. All real-valued features as well as the regression output were standardized before modeling (with the test predictions restored to their original range before calculating final metrics). Overall dataset statistics are listed in Table 1 and further processing steps are given in Section 4.

#### B.1.2. MITV PREPROCESSING

As described in Section B.1.1 and Table 1, the MITV dataset comes with 8 input features, among which 3 are categorical.

<sup>4</sup>provided by OpenWeatherMap

Here we list the relevant parsing and encoding steps used in our setup. The raw time stamp information was parsed to extract additional features such as day of the week, day of the month, year-day fraction, etc. Table 4 shows the corresponding list. Standardization was performed on the input as well as output, as per Table 4, whereby the model predictions were transformed to their original range before calculating final metrics.

#### B.1.3. SPE9 RESERVOIR PRODUCTION RATES (SPE9PR)

This dataset originates from an application of oil reservoir modeling. A reservoir model (RM) is a space-discretized approximation of a geological region subject to modeling. Given a sequence of drilling actions (input), a physics-based PDE-solver (simulator) is applied to the RM to generate sequences of future production rates (oil, gas, water production), typically over long horizons (Killough, 1995). The objective is to train a DNN and accurately predict outputs on unseen input sequences. We used the publicly available SPE9<sup>5</sup> RM, considered a reference for benchmarking reservoir simulation in the industry, and an open-source simulator<sup>6</sup> to produce 28,000 simulations, each with 100 randomized actions (varying type, location, and control parameters of a well) inducing production rate sequences over a span of 25 years, in 90-day increments, i.e., 100 time steps. Furthermore, the RM was partitioned into two regions, A and B. While most of the actions are located in the region A, we also generated 1000 sequences with actions located in the region B thus creating a large degree of mismatch between training and test. The test condition in region B will be referred to as “drift” scenario.

#### B.1.4. SPE9PR PREPROCESSING

The Table 5 lists details on the SPE9PR features (also refer to Section B.1.3 and Table 1). The SPE9PR dataset contains input sequences of actions and output sequences of production rates. An action (feature `type_of_well`), at a particular time, represents a decision whether to drill, and if so, what type of well to drill (an injector or a producer well), or not to drill (encoded by “0”), hence the cardinality is 3. In case of a drill decision, further specifications apply, namely the x- and y-location on the surface of the reservoir, local geological features at the site, and well control parameters. There are 15 vertical cells in the SPE9 each coming with 3 geological features (rel. permeability, rel. porosity, rock type), thus the local geology is a 45-dimensional feature vector at a particular  $(x, y)$  location. Finally, every well drilled so far may be controlled by a parameter called

<sup>5</sup><https://github.com/OPM/opm-data/blob/master/spe9/SPE9.DATA>

<sup>6</sup><https://opm-project.org/>

”Bottom-Hole Pressure” (BHP). Since we provision up to 100 wells of each of the two types, a 200-dimensional vector arises containing BHP values for these wells at any given time. Standardization was performed on the input as well as output as specified in Table 5 whereby the model predictions were transformed to their original range before calculating and reporting final metrics.

## B.2. Training Setup

### B.2.1. HYPERPARAMETERS

Hyperparameters have been determined in two ways: (1) learning rate, regularization, batch, and LSTM size were adopted from an unrelated experimental study performed on a modified reservoir SPE9 (Anonymized), (2) We used DEV2 to determine the dropout rates in the DOMS model. The value  $\beta = 0.5$  was chosen ad-hoc (as a midpoint between pure base and pure meta loss) without further optimization.

### B.3. Implementation Notes

All DNNs were implemented in Tensorflow 1.11. Training was done on a Tesla K80 GPU, with total training time ranging between 3 (MITV) and 24 (SPE9PR) hours. The GARCH Python implementation provided in the `arch` library was used.

## C. Additional Results

### C.1. Individual Metrics

For a more detailed view of the averages in Table 2, we show a split by the individual metrics in Table 7, and, for the SPE9PR which has a total of four output variables, a split by the individual variables in Table 8.

### C.2. Additional Visualizations

In addition to the sample visualizations shown in Section 2 for the JMS, JMV, and JMA systems, here we show some sections of the data and visualize output of all systems. Figures 7 and 8 show the first simulation in the test set of the SPE9PR dataset for the drift and non-drift condition and all its output components, respectively. Figures 9 and 10 show the output on the MITV drift and non-drift condition, respectively. For each model, a miss rate value of 0.1 across the entire test set was used in the visualizations.

#### C.2.1. INTERACTIVE NOTEBOOK

We also provide an interactive notebook that allows for inspecting all system output on an arbitrary portion of the test data in both the non-drift and drift condition. Please refer to the README file within the zip-file uploaded as

the Supplementary Material part of our submission.

#### C.2.2. JMV VARIANCE TUNING ON DEV DATA

Section 4 lists individual training steps for each system. It is noted that the meta-modeling arrangements have used the DEV partition for tuning in a final step. The motivation for using a partition not included in training the base model is the avoidance of meta-training on biased targets, i.e., targets generated by the base model on its own training data. In this context, a question arises whether a similar tuning step could help the JMV model. We followed the training steps described in Section 4 and then updated the network nodes tied to the variance parameter while keeping the rest of the network fixed. The Table 9 shows the results on the MITV dataset. It seems the benefit of the tuning step does not materialize. In all but the cross-validated drift case the gain decreases (albeit insignificantly) when applying the DEV-only tuning. We conjecture that the benefit of the tuning step exists with the meta-model because of the direct supervision of the meta-model’s prediction. In contrast, the variance in the JMV setting is learned implicitly and may not suffer from the ”biased-target” problem mentioned above.

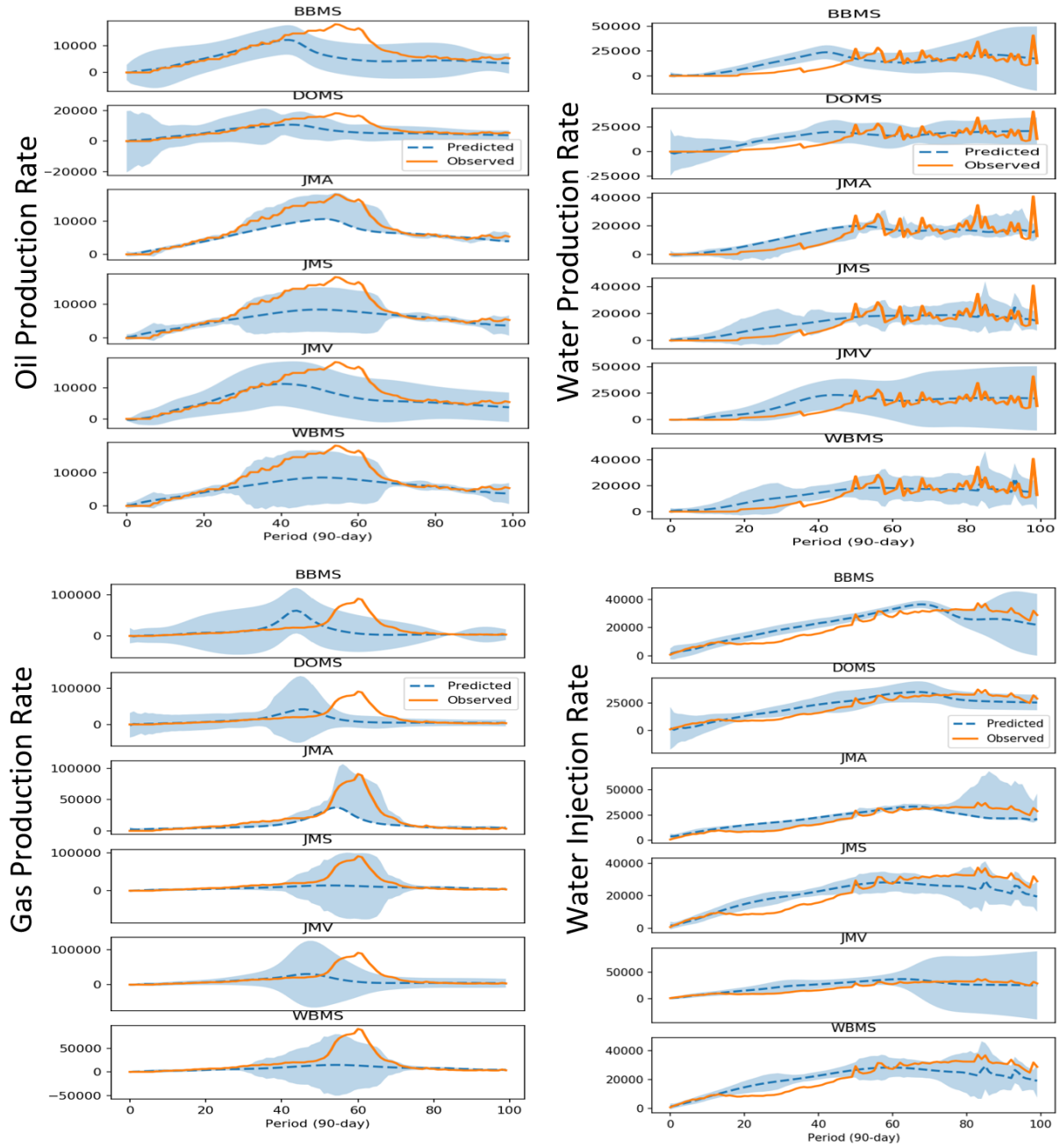


Figure 7. Sample from SPE9PR (simulation 0, drift condition), all components and systems shown.

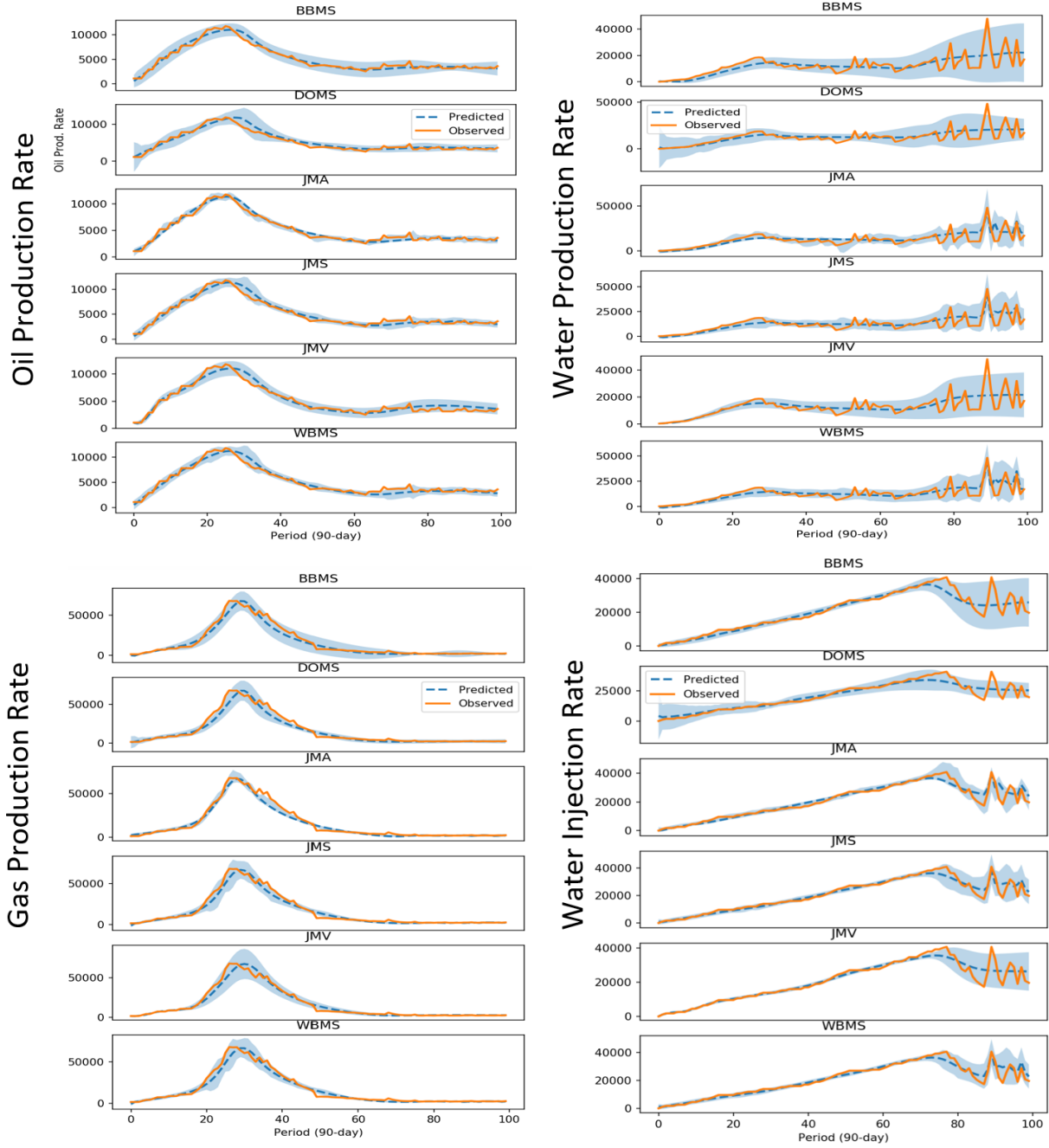


Figure 8. Sample from SPE9PR (simulation 0, non-drift condition), all components and all systems shown.

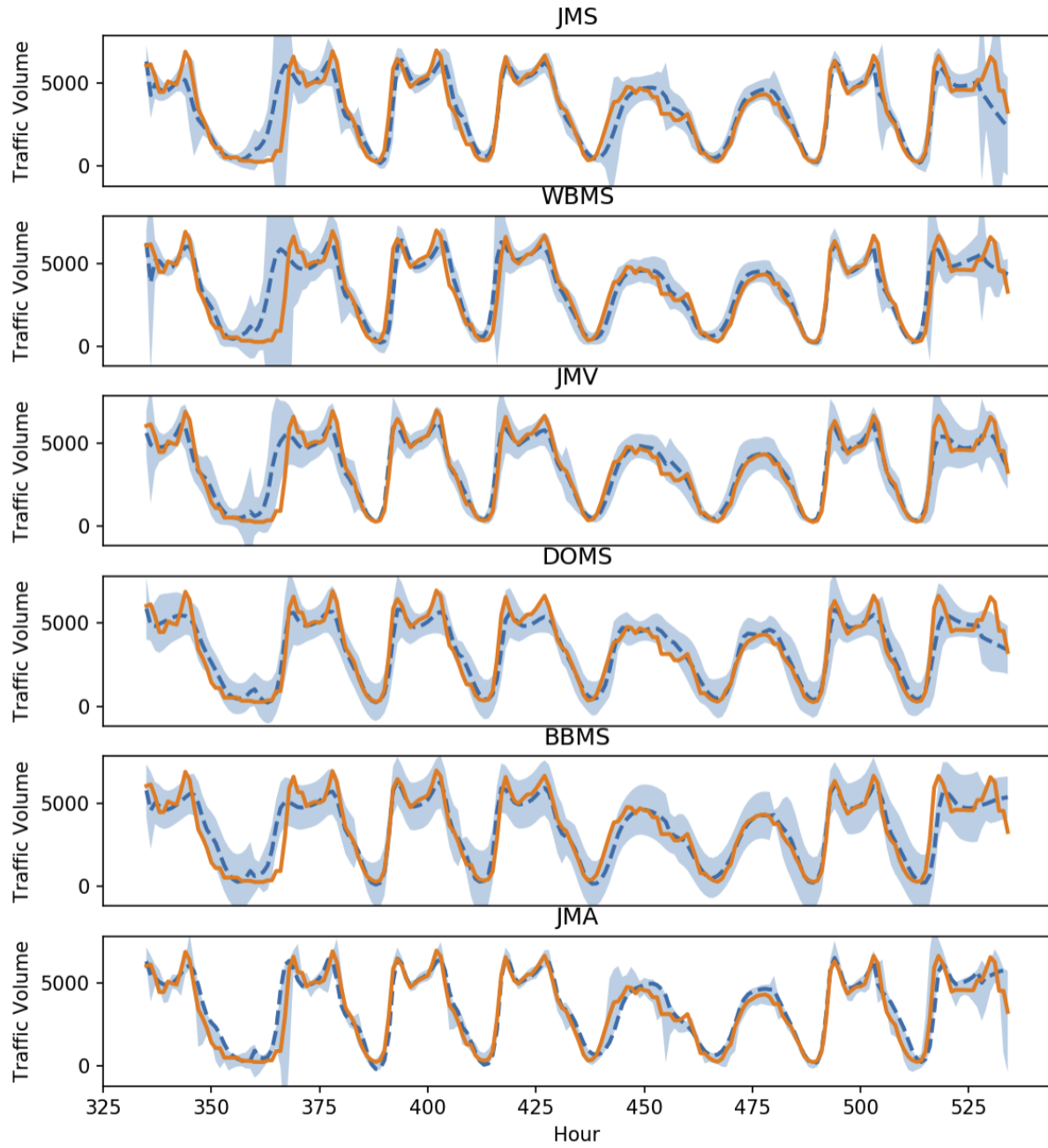


Figure 9. Sample from MITV (drift condition), all systems shown.

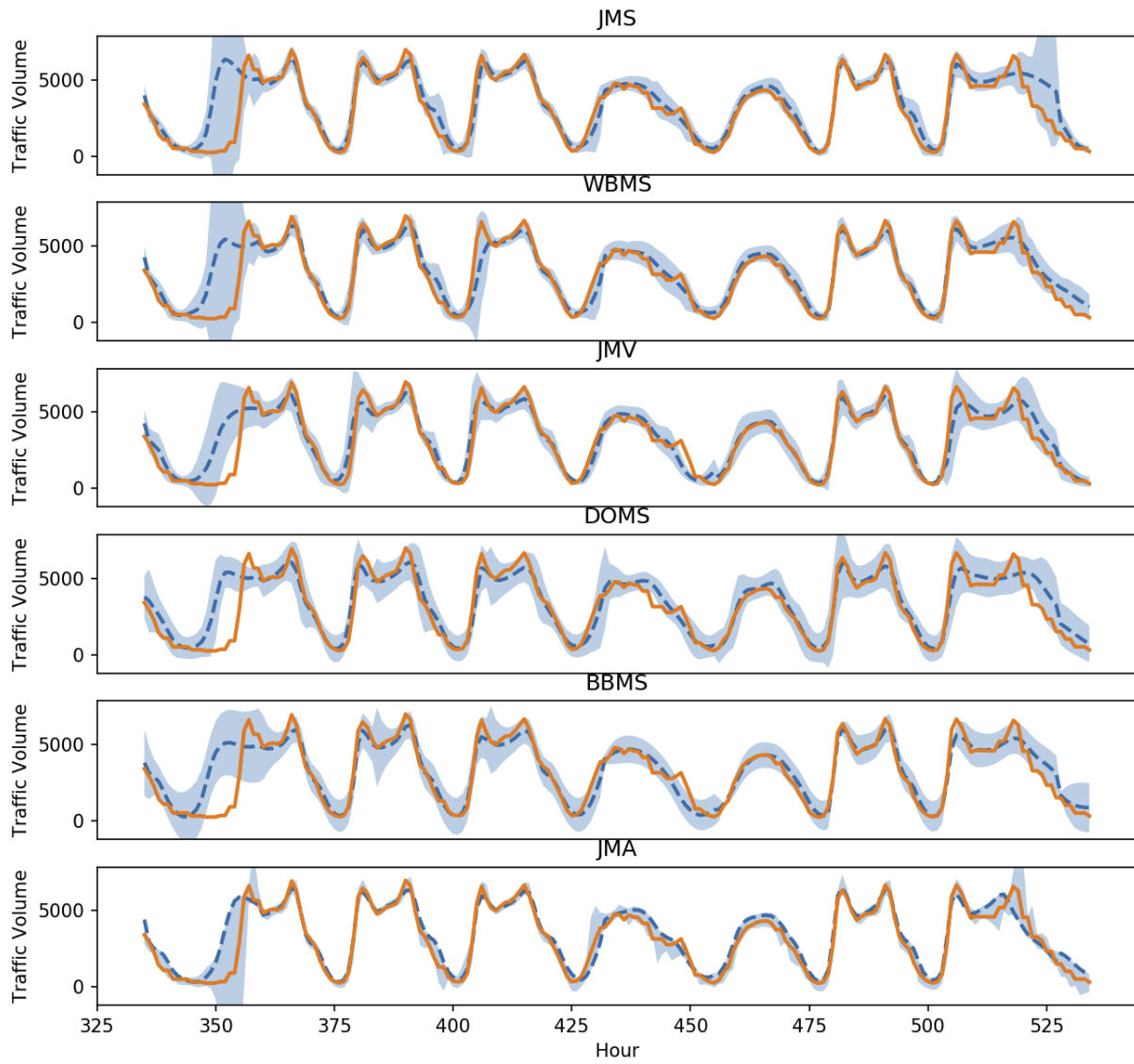


Figure 10. Sample from MITV (non-drift condition), all systems shown.

Table 4. MITV Input and Output Specifications

Feature Name	Range	Categorical	Embedding Dimension	Standardized	Final Dimension
INPUT					
day_of_month	integer $\in [0, 30]$	Y	3	N	3
day_of_week	integer $\in [0, 6]$	Y	3	N	3
month	integer $\in [0, 11]$	Y	3	N	3
frac_yday	real $\in [\frac{1}{365}, 1]$	N	-	Y	1
weather_type	integer $\in [0, 10]$	Y	3	N	3
holiday_type	integer $\in [0, 11]$	Y	3	N	3
temperature	real $\in \mathbb{R}$	N	-	Y	1
rain_1h	real $\in \mathbb{R}_0^+$	N	-	Y	1
snow_1h	real $\in \mathbb{R}_0^+$	N	-	Y	1
clouds_all	real $\in [0, 100]$	N	-	Y	1
<b>Total</b>					<b>20</b>
OUTPUT					
traffic_volume	real $\in \mathbb{R}_0^+$	N	-	Y	1
<b>Total</b>					<b>1</b>

Table 5. SPE9PR Input and Output Specifications

Feature Name	Range	Categorical	Embedding Dimension	Standardized	Final Dimension
INPUT					
type_of_well	integer $\in \{0, 1, 2\}$	Y	3	N	3
location_x	integer $\in [0, 24]$	Y	10	N	10
location_y	integer $\in [0, 25]$	Y	10	N	10
vertical_geology	real $\in \mathbb{R}^{45}$	N	-	Y	45
per_well_control	real $\in \mathbb{R}^{200}$	N	-	Y	200
<b>Total</b>					<b>258</b>
OUTPUT					
oil_prod_field_rate	real $\in \mathbb{R}_0^+$	N	-	Y	1
gas_prod_field_rate	real $\in \mathbb{R}_0^+$	N	-	Y	1
water_prod_field_rate	real $\in \mathbb{R}_0^+$	N	-	Y	1
water_inj_field_rate	real $\in \mathbb{R}_0^+$	N	-	Y	1
<b>Total</b>					<b>4</b>

Table 6. Hyperparameter settings

<b>Hyper-parameter</b>	<b>Where used</b>	<b>Value</b>	<b>Comment</b>
Learning rate	all	0.001	Stage 1 training
Learning rate	all	0.0002	Stage 2 training, see Section 4
Batch size	all	100	
$L_2$ penalty coefficient	all, except DOMS	0.0001	
$L_2$ penalty coefficient	DOMS	0.0	
Dropout	DOMS	0.25/0.1/0.25	LSTM Input/State/Output (encoder and decoder)
Base LSTM size	all	32	
Meta LSTM size	meta models	16	
$\beta$ in Eq. (1)	1.0/0.5/0.0	see Section 4	

**Uncertainty Prediction for Deep Sequential Regression Using Meta Models**

Table 7. Symmetric gains split by individual metric (compare to Table 2)

<b>Model</b>	<b>Deficit@0.01</b>	<b>Deficit@0.05</b>	<b>Deficit@0.1</b>	<b>Excess@0.01</b>	<b>Excess@0.05</b>	<b>Excess@0.1</b>	<b>MinCost</b>	<b>Average</b>
<i>%G*</i> , MITV "Non-Drift" Scenario								
JMS	61.3	74.8	75.6	64.5	54.6	40.1	33.9	57.8
WBMS	48.0	73.8	74.3	62.7	50.7	35.1	32.3	53.8
JMV	-33.9	31.9	32.5	35.8	31.4	28.2	16.8	20.4
ENSMB	19.9	50.5	50.9	10.4	-8.9	-29.1	10.0	14.8
DOMS	28.1	24.8	23.1	11.5	3.3	-1.6	2.8	13.1
BBMS	9.7	27.9	16.3	-18.8	-18.7	-18.7	-0.8	-0.4
<i>%G<sup>xval</sup></i> , MITV "Non-Drift" Scenario								
JMS	75.9	78.1	77.4	58.0	51.9	39.6	33.9	59.3
WBMS	67.4	79.6	77.7	57.7	42.7	29.8	32.3	55.3
JMV	4.4	38.9	35.8	29.1	27.1	26.3	16.8	25.5
ENSMB	28.0	48.3	48.7	7.4	-4.0	-18.8	9.9	17.0
DOMS	78.2	63.9	62.3	-35.7	-32.4	-49.2	2.8	12.8
BBMS	61.6	21.5	15.4	-61.0	-12.5	-15.9	-0.9	1.2
<i>%G*</i> , MITV "Drift" Scenario								
JMS	40.5	78.0	77.5	57.7	45.0	31.9	36.7	52.5
WBMS	18.4	68.8	70.8	43.6	32.8	15.6	25.8	39.4
JMV	-3.8	29.0	30.9	23.0	25.5	21.6	13.8	20.0
ENSMB	-41.2	38.3	45.2	9.4	8.7	-1.8	14.1	10.4
DOMS	23.4	23.7	24.7	11.6	14.2	11.4	7.3	16.6
BBMS	-38.2	5.7	8.7	-11.8	-12.2	-14.1	-0.2	-8.9
<i>%G<sup>xval</sup></i> , MITV "Drift" Scenario								
JMS	71.7	81.6	80.1	53.2	39.1	27.1	36.7	55.6
WBMS	67.9	79.2	78.5	22.9	19.4	2.0	25.8	42.3
JMV	-27.2	28.5	32.7	29.1	25.9	19.6	13.8	17.5
ENSMB	-78.4	35.2	44.7	17.0	10.6	0.0	13.7	6.1
DOMS	38.4	18.9	23.4	2.8	16.6	13.3	7.4	17.3
BBMS	6.2	13.2	13.1	-17.5	-17.4	-18.6	-0.3	-3.0
<i>%G*</i> , SPE9PR "Non-Drift" Scenario								
JMS	55.7	55.8	56.8	46.1	42.5	37.7	30.8	46.5
WBMS	50.9	54.5	55.6	47.4	41.5	35.4	28.5	44.8
JMV	50.5	54.2	53.7	51.8	43.3	37.0	26.4	45.3
ENSMB	39.9	43.8	44.6	4.9	4.0	-3.0	14.4	21.2
DOMS	7.1	10.2	10.4	-6.9	-5.8	-6.8	1.0	1.3
BBMS	51.0	52.6	50.0	25.1	18.2	10.6	15.7	31.9
<i>%G<sup>xval</sup></i> , SPE9PR "Non-Drift" Scenario								
JMS	56.8	56.5	57.0	45.7	42.0	37.4	30.8	46.6
WBMS	50.7	54.9	56.2	47.5	41.2	34.9	28.5	44.8
JMV	51.4	56.0	55.2	51.6	42.3	35.5	26.4	45.5
ENSMB	27.2	42.5	44.6	11.0	5.3	-2.9	14.4	20.3
DOMS	7.7	9.5	10.1	-7.0	-5.3	-6.4	1.0	1.4
BBMS	76.4	61.2	54.8	-11.5	10.6	5.0	15.7	30.3
<i>%G*</i> , SPE9PR "Drift" Scenario								
JMS	65.4	69.0	68.4	52.6	50.0	46.3	44.5	56.6
WBMS	63.7	68.0	66.9	53.5	48.1	41.8	39.5	54.5
JMV	29.2	22.7	21.9	-33.9	-42.8	-52.9	10.3	-6.5
ENSMB	25.1	28.4	29.6	-31.6	-14.4	-10.4	14.8	5.9
DOMS	-1.4	9.4	12.0	-10.7	-4.5	-8.5	2.7	-0.1
BBMS	19.4	33.8	31.0	-7.6	1.1	-3.0	6.7	11.6
<i>%G<sup>xval</sup></i> , SPE9PR "Drift" Scenario								

**Uncertainty Prediction for Deep Sequential Regression Using Meta Models**

---

Table 8. Symmetric gains split by individual components - SPE9PR only (compare to Table 2). OPR=Oil Production Rate, WPR=Water Production Rate, GPR=Gas Production Rate, WIN=Water Injection Rate.

Model	$E_{base}$					Excess-Deficit				
	OPR	WPR	GPR	WIN	Average	OPR	WPR	GPR	WIN	Average
$\%G^*$ , SPE9PR "Non-Drift" Scenario										
JMS	0.12	0.28	0.17	0.09	0.17	18.25	66.45	53.60	47.61	46.48
WBMS	0.12	0.28	0.17	0.09	0.16	17.78	62.08	52.43	47.03	44.83
JMV	0.10	0.29	0.16	0.09	0.16	6.67	74.50	43.74	56.24	45.29
DOMS	0.12	0.31	0.18	0.11	0.18	-6.88	0.68	21.64	-10.16	1.32
BBMS	0.12	0.30	0.16	0.10	0.17	-3.85	74.44	16.89	40.08	31.89
$\%G^*$ , SPE9PR "Non-Drift" Scenario										
JMS	0.12	0.28	0.17	0.09	0.17	19.13	66.98	52.18	48.19	46.62
WBMS	0.12	0.28	0.17	0.09	0.16	18.32	62.60	51.07	47.39	44.85
JMV	0.10	0.29	0.16	0.09	0.16	6.92	75.74	43.12	56.23	45.50
DOMS	0.12	0.31	0.18	0.11	0.18	-6.56	0.46	21.94	-10.27	1.39
BBMS	0.12	0.30	0.16	0.10	0.17	-3.84	76.80	7.71	40.63	30.33
$\%G^*$ , SPE9PR "Drift" Scenario										
JMS	0.28	0.30	0.45	0.13	0.29	49.97	24.13	119.73	32.54	56.59
WBMS	0.31	0.34	0.45	0.14	0.31	51.49	27.09	102.64	36.77	54.50
JMV	0.30	0.32	0.51	0.20	0.33	1.12	-6.18	26.99	-47.96	-6.51
DOMS	0.28	0.28	0.45	0.11	0.28	-20.24	-6.97	22.32	4.31	-0.15
BBMS	0.32	0.31	0.54	0.13	0.33	-4.18	-1.04	26.64	25.13	11.64
$\%G^{xval}$ , SPE9PR "Drift" Scenario										
JMS	0.28	0.30	0.45	0.13	0.29	61.81	39.10	74.23	27.01	50.54
WBMS	0.31	0.34	0.45	0.14	0.31	59.11	34.21	60.51	21.51	43.84
JMV	0.30	0.32	0.51	0.20	0.33	2.15	9.15	19.51	-13.28	4.38
DOMS	0.28	0.28	0.45	0.11	0.28	0.81	-27.32	15.73	-10.09	-5.22
BBMS	0.32	0.31	0.54	0.13	0.33	2.55	4.67	20.74	23.36	12.83

Table 9. Relative optimum and cross-validated gains using Excess-deficit metrics for the JMV system without (JMV) and with (JMV- $\sigma$ ) variance tuning on DEV. Elements marked<sup>†</sup> within same column are in a statistical tie.

<b>Evaluation</b>	$\%G^*$	$\%G^x$
JMV (Drift)	20.0	17.5 <sup>†</sup>
JMV- $\sigma$ (Drift)	15.0	19.4 <sup>†</sup>
JMV (Match)	20.4 <sup>†</sup>	25.5
JMV- $\sigma$ (Match)	16.2 <sup>†</sup>	16.9